Comparison of various high-stress wear conditions and wear performance of martensitic steels

Kati Valtonen[1]*, Niko Ojala[1,2], Oskari Haiko[3], and Veli-Tapani Kuokkala[1]

[1]Tampere University, Faculty of Engineering and Natural Sciences, Chemistry and Materials Science, Tampere Wear Center, Tampere, Finland

[2]Robit Ltd, Lempäälä, Finland

[3]University of Oulu, Faculty of Technology, Materials Engineering, Oulu, Finland

*Corresponding author: Kati Valtonen; Tampere University, Tampere Wear Center, P.O.Box 589, FI-33101 Tampere, Finland; p. +358 40 849 0142; email kati.valtonen@tut.fi

ABSTRACT

The demanding environments typically encountered by the wear resistant steels create challenges for the materials selection, because the hardness grades of the steels alone do not reveal the true nature of their wear behavior. In this study, five commercial wear resistant steels were tested using three application oriented test methods with five different test variables for abrasion, impact-abrasion, and slurry erosion. All the used test methods produced high-stress conditions that crushed the used mineral abrasive, plastically deformed the sample surfaces, and led to the formation of adiabatic shear bands. When the results produced by the chosen methods were compared, the normalization of the wear losses by the wear area and test time revealed well the differences between the methods. The test methods ranked the steels similarly, but there were clear differences in the wear rates and wear mechanisms between the tests. In addition, the abrasive methods produced surface adiabatic shear bands, while subsurface shear bands were initiated by the more impacting methods. In the studied conditions, the work hardening ability of the steel had a clear influence on its wear resistance, which largely explains the marked differences in the wear rates of the studied commercial 500HB grade steels.

Keywords: Wear testing; steel; abrasion; impact wear

1. Introduction

The martensitic wear resistant steels are typically used in various challenging high-stress wear conditions, such as mineral haulage and crushing, slurry transportation, dredging, demolition of concrete structures, and forest industry. In many applications, the wear environment is very complex and contains different wear mechanisms. Moreover, the wear resistant steels are not standardized and the generally used hardness based grading does not completely describe nor predict their wear behavior [1]. Thus, well-planned and multifaceted application oriented wear testing of the steels as a part of the material selection process is highly recommended for achieving a proper correlation to practical applications.

The widely used standardized rubber wheel abrasion testers [2] are not able to produce similar plastic deformation and work hardening in the steels as the high-stress in-service conditions [3–6]. Therefore, various tests methods have been developed for the testing of high-stress abrasive or impact-abrasive wear of materials with natural mineral abrasives [7–14]. This kind of application oriented wear test methods are typically non-standardized, but their versatility and the possibility to adjust the test parameters make them well suited for the simulation of a wide range of in-service applications [15–18]. These methods can be used, for example, to simulate mineral handling and processing [7,12,13,16], crushing applications in mining [8,9,12], slurry pumps [10], tunnel boring machines [11], and high-temperature environments [14].

Ojala et al. [1] compared the high-stress abrasion behavior of 15 commercial 400HB grade wear resistant steels and found over 50% differences in the wear performance of these nominally similar steels. The main reason for the different wear behavior was found in the alloying and manufacturing methods used for the steels, leading to different microstructures and work hardening behavior. Similar results have been reported for example by Sundström et al. [19], who suggested that instead of bulk hardness, the hardness of the plastically deformed wear surface is a better measure of the wear resistance of the steels under impact-abrasion conditions.

There is no straightforward and unambiguous way to compare the wear testing methods involving different wear mechanisms, test times, and sample sizes. Typically, the test results are normalized by the results of a reference material, which is tested either simultaneously or separately with the exactly same method [20]. This in general works

well, when only the materials are being compared. However, when comparing the test methods to each other, also the test parameters, such as the wear area and test duration must be taken into account [16]. In this study, the wear in rather complex high-stress wear environments with natural rock was simulated in the laboratory conditions. Both the test methods and the wear behavior of the selected steels were compared and characterized in order to explain the differences observed in the wear response of commercial steels with nominally same bulk hardness, as well as how the different test methods correlate with each other and with the field tests in the case of martensitic steels.

2. Materials and methods

2.1. Materials

Three commercial 500HB grade quenched and tempered steels were compared using three different test equipment and five different testing procedures. A 400HB steel was used as a reference material, but comparison was also made with a 600HB steel. Table 1 lists the typical properties of the tested steels, including the measured bulk hardness, yield strength ($R_{p0.2}$), ultimate tensile strength (R_m), elongation (A5), and impact toughness at -40°C obtained from the data sheets. The typical carbon equivalent values were determined using equations CEV = C + Mn/6 + (Cr + Mo + V)/5 + (Ni + Cu)/15 and CET = C + (Mn+Mo)/10 + (Cr+Cu)/20 + Ni/40. The martensite start temperatures were calculated with the Andrews' method, M_s(°C) = 512 - 453C - 16.9Ni + 15Cr - 9.5Mo +217C^2 - 71.5CMn - 67.6CCr. The abrasive used in the tests was Finnish granite from Sorila mine (Fig. 2f). Sorila granite contains plagioclase (45 wt%), quartz (25 wt%), orthoclase (13 wt%), biotite (10 wt%) , and amphibole (5 wt%) [21]. The granite was crushed with a jaw crusher in the quarry and sieved for the needed particle size distributions.

Table 1. Typical properties of the studied steels.

Steel	**A400**	**B500**	**C500**	**D500**	**E600**
Hardness HV10 [kg/mm^2]	421 ± 11	493 ± 6	497 ± 3	486 ± 5	634 ± 5
$R_{p0.2}$ [N/mm^2]	1000	1250	1250	1300	1650
R_m [N/mm^2]	1250	1600	1550	1600	2000
A5 [min %]	10	8	8	9	7
Impact toughness -40°C [J]	30	30	37	n/a	20
CEV	0.41	0.57	0.63	0.58	0.73
CET	0.28	0.40	0.43	0.38	0.55
Ni+Mo [wt%]	0.17	0.60	0.78	0.20	<2.8
Total amount of alloying elements [wt%]	2.05	3.30	3.26	3.49	n/a
M_s [°C]	439	385	379	397	n/a

Plate thickness [mm]	10	38	38	38	30

2.2. Wear test methods

Fig. 1 shows the schematics of the three different wear test systems used in this work, i.e., the crushing pin-on-disc, the high-speed slurry-pot, and the impeller-tumbler. Five different test procedures, presented in Table 2, were used to produce different high-stress wear conditions, where the used granite abrasive becomes crushed to smaller particles.

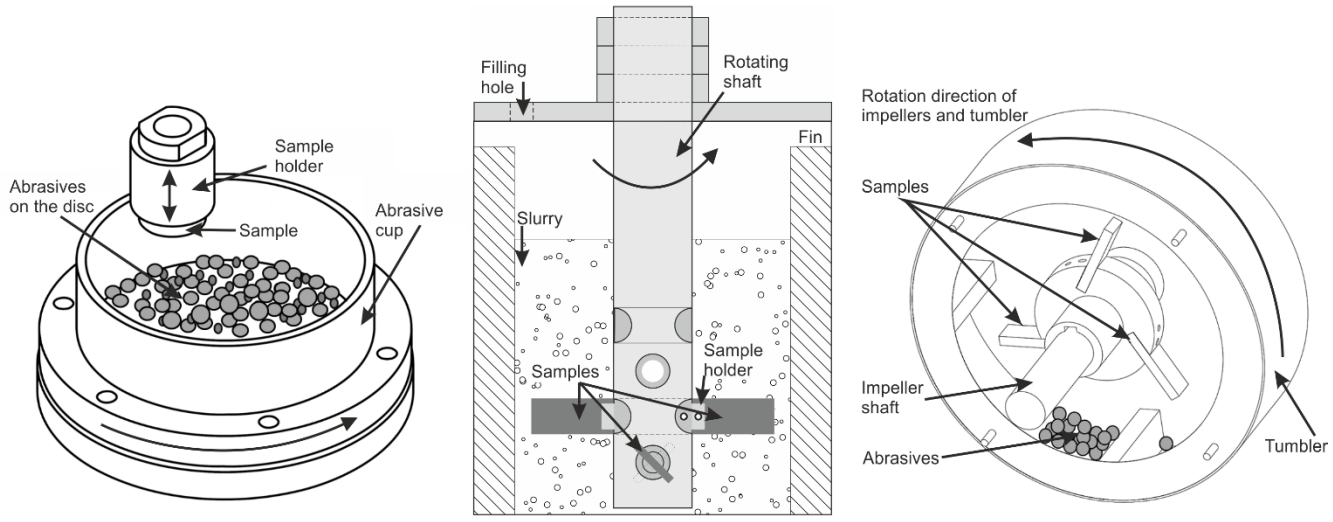

a) *b)* *c)*

Fig. 1. Schematics of the used test methods: a) crushing pin-on-disc, b) high-speed slurry-pot, and c) impeller-tumbler.

Table 2. Test parameters used in the wear tests.

Test method	**Crushing pin-on-disc**		**High-speed slurry-pot**	**Slurry-pot with dry abrasive bed**	**Impeller-tumbler**
Abbreviation	CPOD with 450HB disc	CPOD with S355 disc	Slurry-pot	Dry-pot	Impeller-tumbler
Contact time [min]	20		2 x 10	2 x 30	4 x 15
Wear area [mm²]	1017		2540	2540	1200
Sample size [mm]	∅ 36 x 35		60 x 44 x 5.6	60 x 44 x 5.6	75 x 25 x 10
Number of samples	1		4	2	3
Normal force [N]	200	240			
Disc material	450HB	S355			
Reference material			A400	A400	A400
Sample angle [°]	0		45	45	60
Speed at sample tip [m/s]			15	5	7.7
Travel length [m]	123		17 900	17 900	27 700
Abrasive	Sorila granite		Sorila granite	Sorila granite	Sorila granite
Abrasive size [mm]	2-10		8-10	8-10	10-12.5

Amount of abrasive in one test cycle [g]	500	3000	9000	900
Running-in	15 min	-	-	15 min

In the crushing pin-on-disc (CPOD) tests [1,20], a cylindrical sample is pressed cyclically against a rotating gravel bed on a 160 mm steel disc (Fig. 1a). The sample is able to rotate freely about its axis during the compression cycle and therefore the sliding direction is constantly changing. Two test procedures were used. In the first procedure, the disc material was a 450HB martensitic wear resistant steel, and the applied compression force was about 200 N. In the second procedure, the effect of a softer plate material was studied using a S355 structural steel disc with a hardness of 200 HV and 240 N compression force. The rotation speed in both of these test types was 28 rpm.

In the high-speed slurry-pot tests [22], four samples were attached at a +45° tilt angle to the rotating vertical shaft (Fig. 1b). The samples were tested for 20 minutes at the rotational speed of 1500 rpm, which produces a circumferential speed of 15 m/s at the tip of the samples. The slurry concentration was 33 % in all of these tests. When the device was used with dry gravel (dry-pot) [17], the two samples were attached to the shaft at the second lowest level and the test chamber was filled with granite gravel. The samples were tested for 60 minutes at 500 rpm, corresponding to the speed of 5 m/s at the tip of the samples. In both types of tests, i.e., slurry-pot and dry-pot tests, the travel length was the same 17,900 m, and the position of the samples was changed with the abrasive in the mid-point of the test cycle.

In the impeller-tumbler tests [23], three samples were attached as impellers to the rotating horizontal shaft at a 60° tilt angle (Fig. 1c).. The rotational speeds of the impellers and the tumbler were 700 rpm and 30 rpm, respectively. Both the impellers and the tumbler were rotating counterclockwise, thus allowing free movement of the abrasive particles. The test time was 60 minutes, and the 10-12.5 mm granite was changed every 15 minutes, because it was crushed and rounded during the tests.

2.3. Characterization methods

The microstructure of the steels, the wear surfaces, and the cross-sections of the samples were characterized by Zeiss Sigma and ULTRAplus field emission gun scanning electron microscopes (SEM). Alicona InfiniteFocus G5 3D profiler was used for the surface roughness analyses, and Keyence VK-X200 laser scanning confocal microscope for revealing

the prior austenite grain boundaries. In addition, optical microscopy and Vickers micro hardness tester Matsuzawa MMT-X7 with a 50 g load (490.3 mN) were used to study the subsurface deformation in the samples. Taper sections with a 17° cut angle were prepared for studying the subsurface adiabatic shear bands in more detail. Samples were polished and etched with Nital (2%) for the microstructural characterizations. The precise compositions of the tested steels were determined using an OBLF QSG 750 optical emission spectrometer.

3. Results

3.1. Characterization of microstructures

The microstructure of all studied steels was martensitic, as depicted in Fig. 2. The three 500HB steels had a quite similar microstructure, but some minor differences could be detected. For example, the amount of white carbide-like precipitates was highest in the C500 steel, probably due to a slightly different tempering treatment, and in the D500 steel, the martensite laths appeared to be shorter and their orientation more random than in the other two HB500 steels, probably due to the smaller prior austenite grain size. Moreover, the amount of precipitates in D500 was smaller compared to the B500 and C500 steels. The microstructure of the B500 steel can be placed somewhere between the two other 500HB steels regarding its tempering/autotempering features. Otherwise, the microstructures and therefore also the mechanical properties of the 500HB steels were found to be quite close to each other.

The microstructures of the A400 and E600 steels, however, differed more from the other materials. The microstructure of the reference steel A400 contained less fresh martensite and more tempered or autotempered martensite. Due to the lower alloying content compared with the other steels, A400 has a higher M_s temperature, and thus it could have been subjected to stronger autotempering during quenching. E600 exhibited a large amount of white carbide-rich areas, resulting from the tempering that had been applied to improve its ductility.

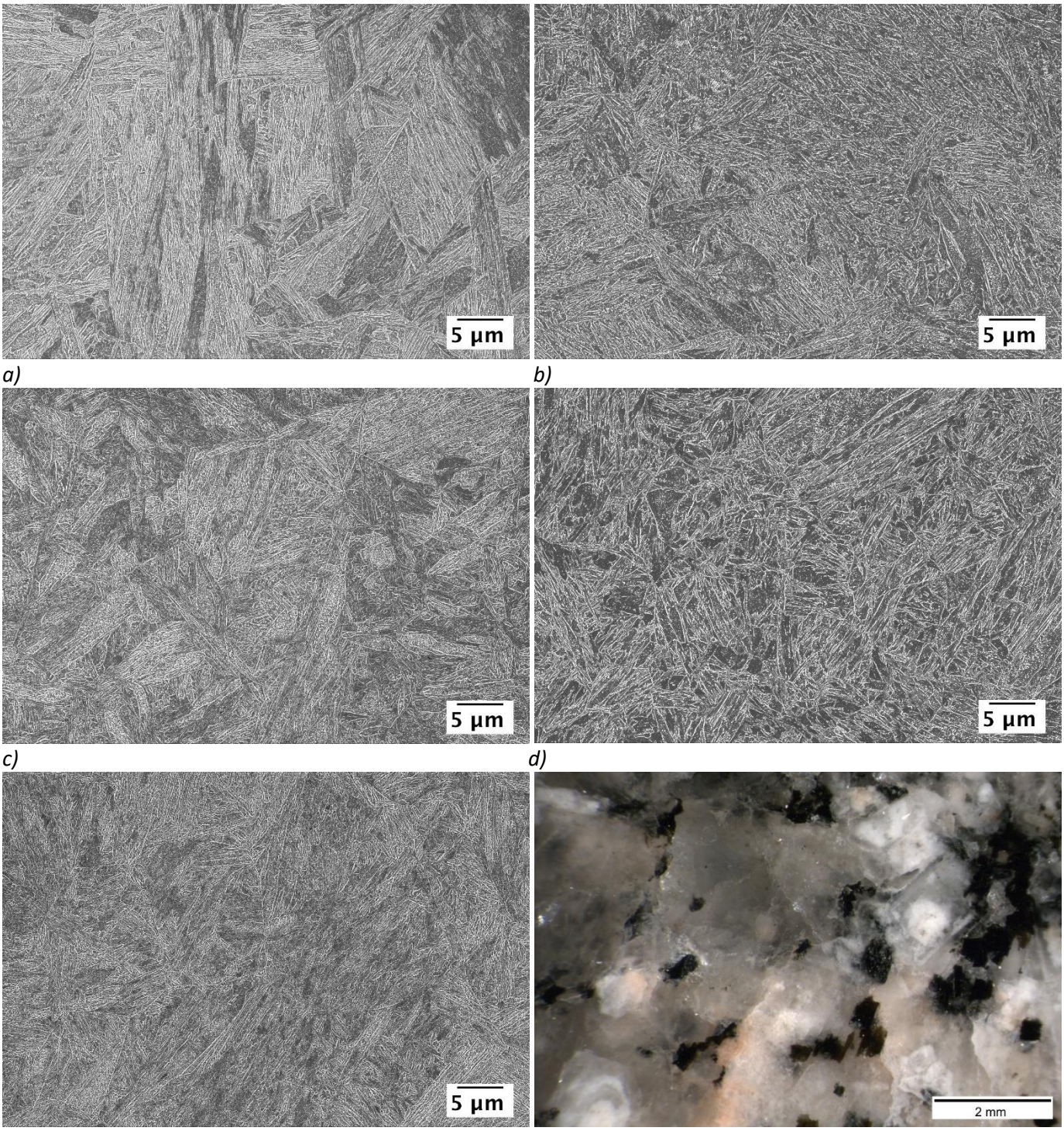

Fig. 2. Microstructures of the tested steels a) A400, b) B500, c) C500, d) D500, e) E600, and the used granite abrasive f) Sorila granite.

The prior austenite grain sizes (PAGS) presented in Table 3 were measured using picric acid etching and laser scanning confocal microscopy. The overall mean linear intercept method by Higginson and Sellars [24] was used for the calculations. D500 had clearly the smallest PAGS (13.0 µm) and the most equiaxed grain structure. However, the distribution of different grain sizes appeared to be more uneven for the D500 steel.

Table 3. Prior austenite grain size measurement results presented with the standard error or 95% confidence limit (overall mean).

Steel	**A400**	**B500**	**C500**	**D500**	**E600**
Normal direction [µm]	16.1±0.7	15.7±0.7	14.2±0.6	12.1±0.5	17.8±0.8
Rolling direction [µm]	22.8±1.0	22.3±1.0	17.5±0.7	13.9±0.5	22.0±1.0
Aspect ratio	1.41	1.42	1.24	1.15	1.23
Overall mean linear intercept [µm]	19.2±1.2	18.7±1.2	15.7±1.0	13.0±0.7	19.8±1.3

3.2. Wear test results

Fig. 3.a presents the average mass losses of the studied steels in the different wear tests, showing that for all steels the absolute mass losses were highest in the slurry-pot tests and lowest in the crushing pin-on-disc tests. The differences between the steel grades, in turn, are shown well in Fig. 3.b, where the mass loss results have been normalized by the mass losses of the A400 reference samples, i.e.:

$$WR_{ND} = \frac{\Delta m_{sample}}{\Delta m_{reference}}$$

In all test types, the D500 samples showed the highest and the E600 samples the lowest wear rates. The crushing-pin-on-disc tests produced the largest differences between the A400 and E600 samples, the difference being almost 60 % in favor of the 600HB grade steel. The difference between A400 and E600 was smallest in the impeller-tumbler tests, ca. 28%.

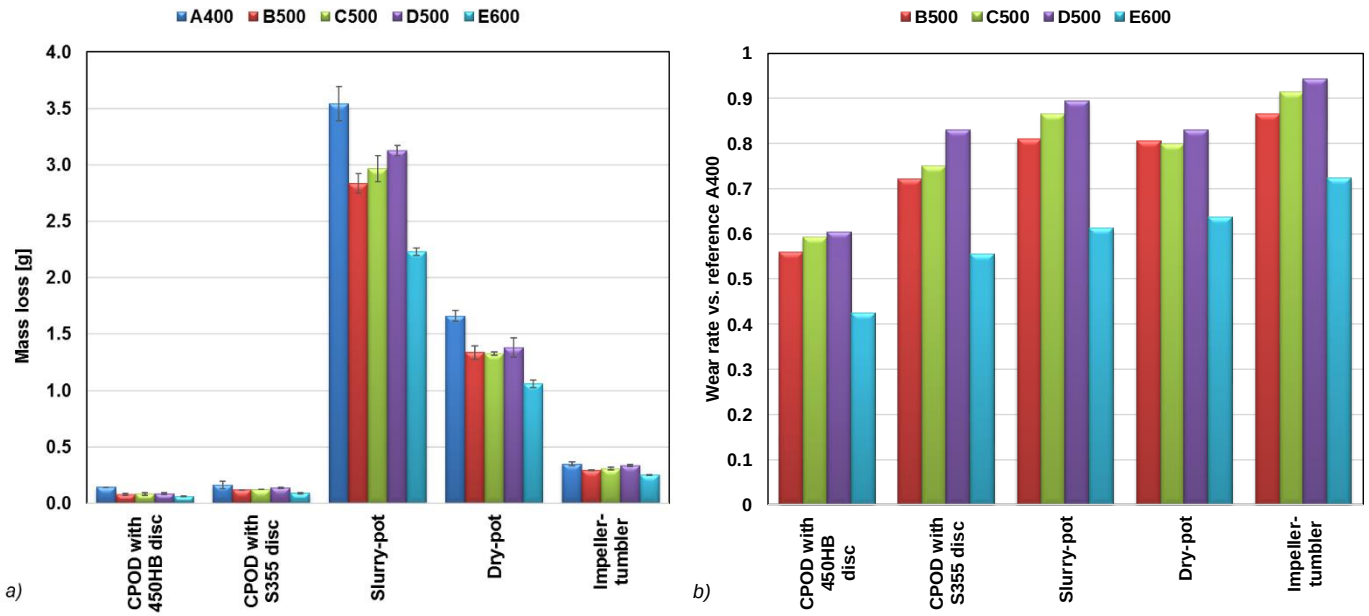

Fig. 3. Wear test results as a) absolute mass loss and b) mass loss/A400 reference. The error bars present the standard deviation.

The simple mass or volume loss results are not suitable for comparing the test methods with varying test parameters. One possibility to compare totally different test methods is to use wear rate $WR_{mm/h}$, where the mass loss of the sample (Δm) is divided by the wear area (A), contact time (t), and density of the steel (ρ), i.e.:

$$WR_{mm/h} = \frac{\Delta m}{t \cdot A \cdot \rho} = \frac{\Delta V}{t \cdot A}$$

Another quite similar method is to use wear rate $WR_{mm/km}$, where the volume loss is correlated to the travel length (ΔL) of the sample instead of the contact time, i.e.:

$$WR_{mm/km} = \frac{\Delta m}{\Delta L \cdot A \cdot \rho} = \frac{\Delta V}{\Delta L \cdot A}$$

Fig. 4 presents the wear rates of the studies steels as $WR_{mm/h}$ and $WR_{mm/km}$. When the wear rates are presented as a function of test time (mm/h), the slurry-pot method with a high rotational speed produces clearly the highest wear rates. However, when the wear losses are correlated to the travel length of the sample during the test, the crushing pin-on-disc with a much slower test speed produces the highest wear rates (mm/km). The impeller-tumbler method gives the lowest wear rates with both ways of presentation.

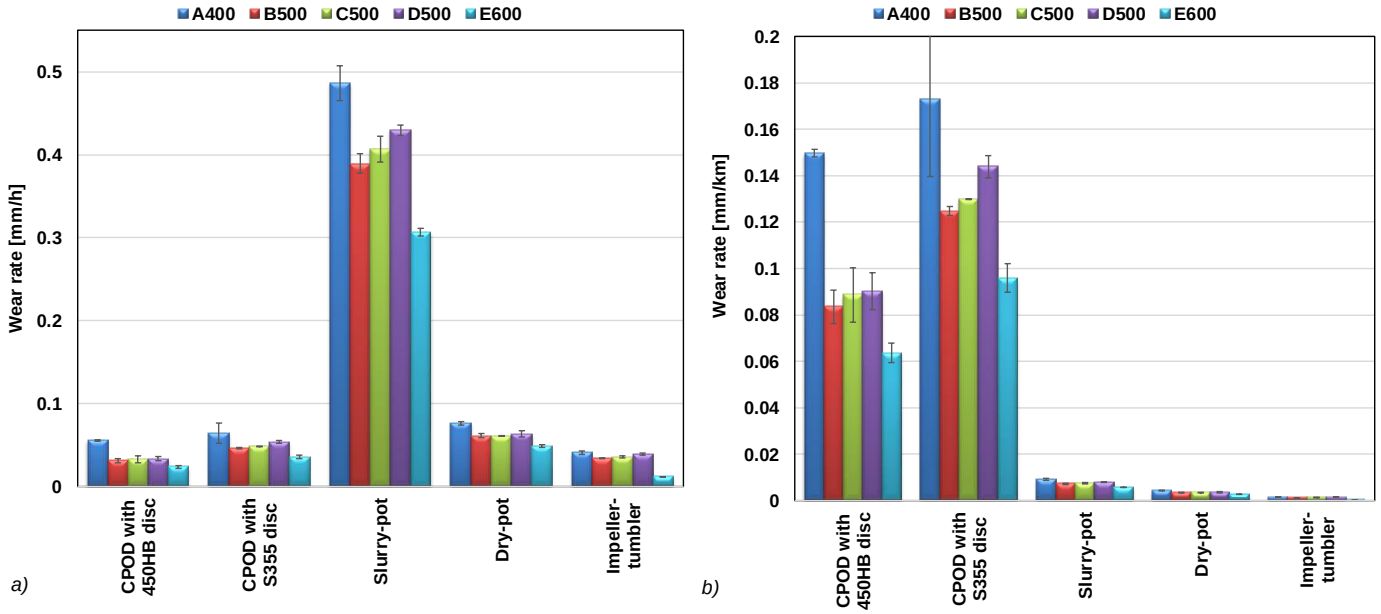

Fig. 4. Wear rates in different test methods presented as the volume loss divided by the wear area and a) the test time and b) the average travel length of the sample in contact with the abrasive. The error bars present the standard deviation.

3.3. Characterization of wear surfaces

The wear surface characterization revealed only minor differences between the studied steel grades but clear differences between the test methods. Fig. 5 presents typical wear surfaces of all studied steels tested with the high-speed slurry-pot. The images are generated by combining secondary electron detector (SE2) and angle selective backscattering electron detector (AsB) signals to enhance the elemental contrast. In the images, the embedded rock therefore appears darker and the steel lighter. There are marked amounts of rock embedded in the steel surfaces, which are also highly deformed. The amounts of plastic deformation and embedded rock decrease with increasing steel hardness, which is also seen from the roughness values shown in Fig. 6a. The wear mechanism in the slurry-pot tests is impact-abrasive, the impacting rock particles heavily scratching and plastically deforming the surfaces.

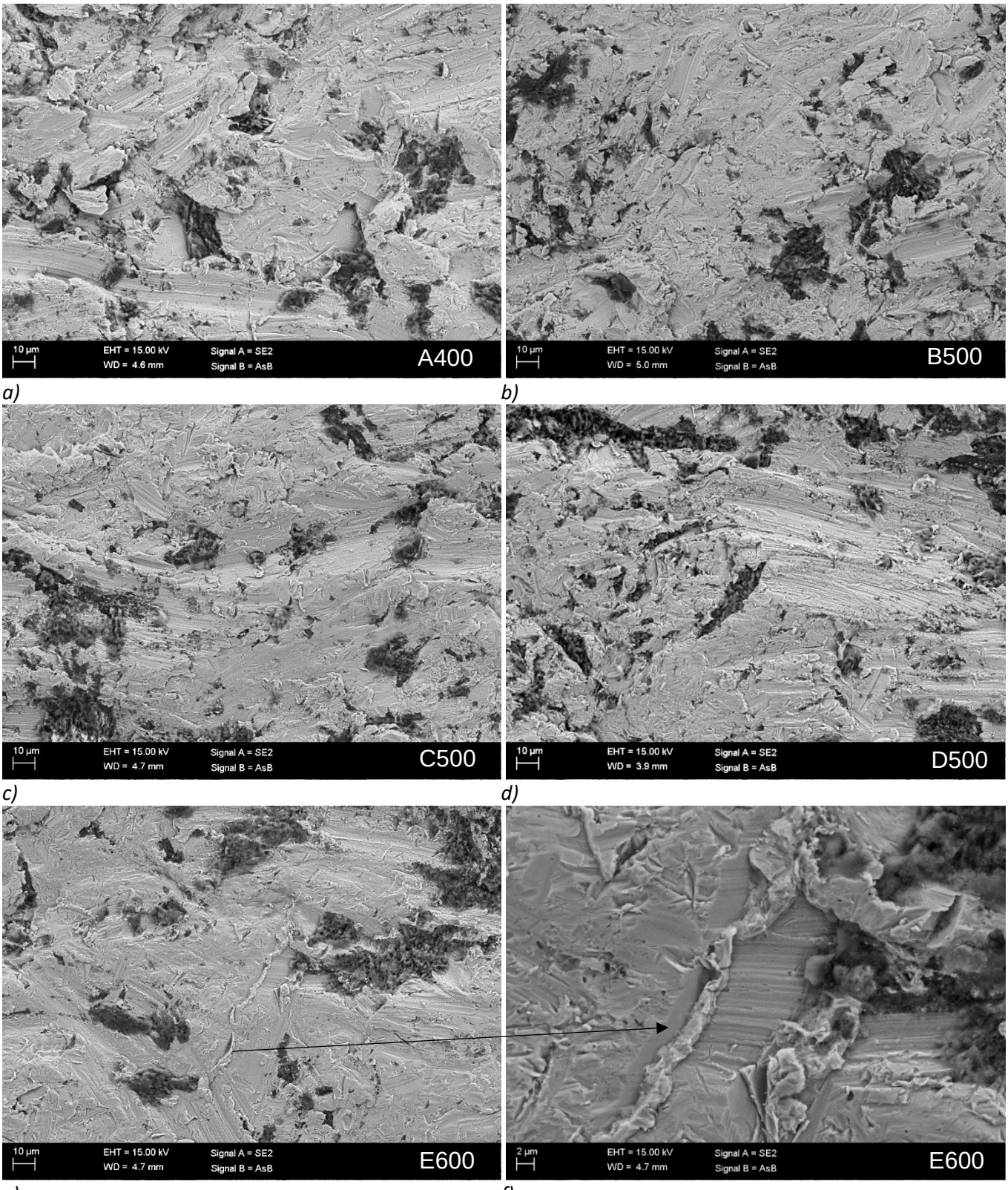

Fig. 5. SEM images comparing the wear surfaces of a) A400, b) B500, c) C500, d) D500, and e, f) E600 steels tested with the high-speed slurry-pot. The arrow from e) to f) points to a typical impact mark on the surface. The abrasives have moved from left to right.

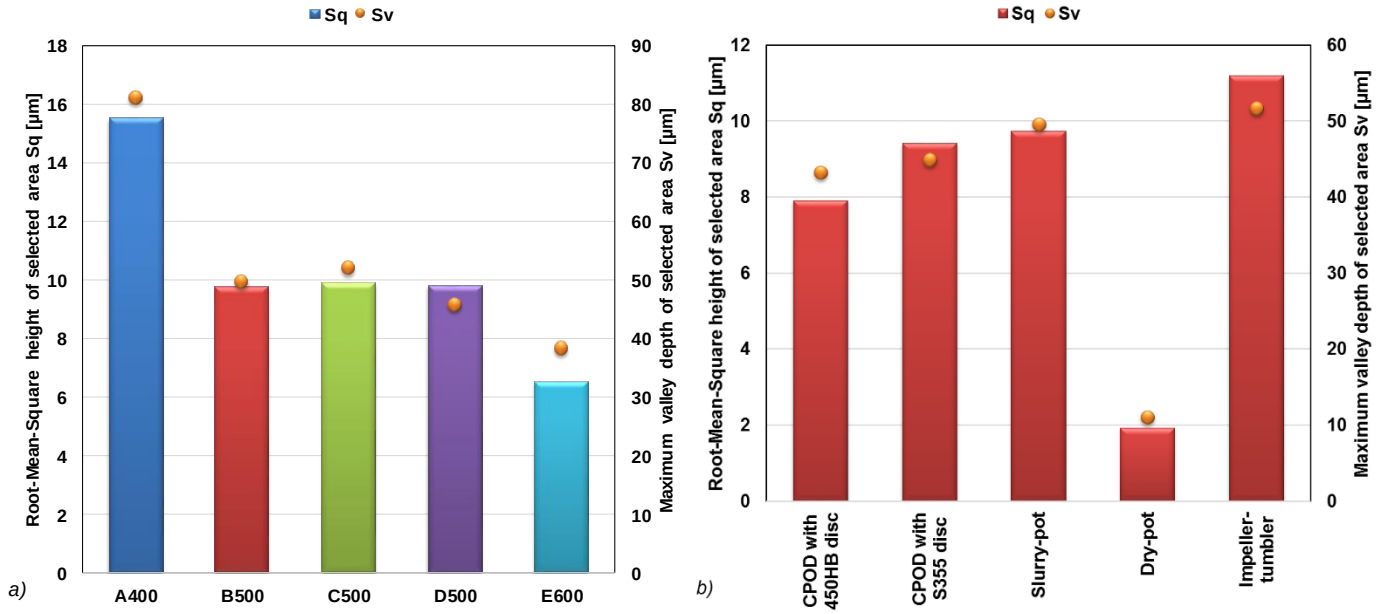

Fig. 6. Roughness values for a) all steels tested with the slurry-pot and b) B500 steel tested with different methods.

Examples of the 500B steel wear surfaces produced by the different test methods are shown in Fig. 7. Although in the crushing pin-on-disc tests the disc does not touch the sample pin, the disc has a marked effect on the wear rate and the appearance of the wear surface. Both CPOD wear surfaces in Figs. 7a and b contain plenty of scratches, but the amount of cutting is higher with the softer structural steel disc, as also the roughness values in Fig. 6b indicate. On the other hand, there are also clear marks of strong deformation and rolling of the rocks between the surfaces, when the disc and the pin have the same hardness. The highest amount of embedded rock was found on the wear surfaces of samples tested with the dry-pot method. Also the surface roughness values were clearly lowest with this test method. The impeller-tumbler wear surfaces were highly deformed and very rough, and as shown in the previous studies [25], micro fatigue is the main wear mechanism in this method.

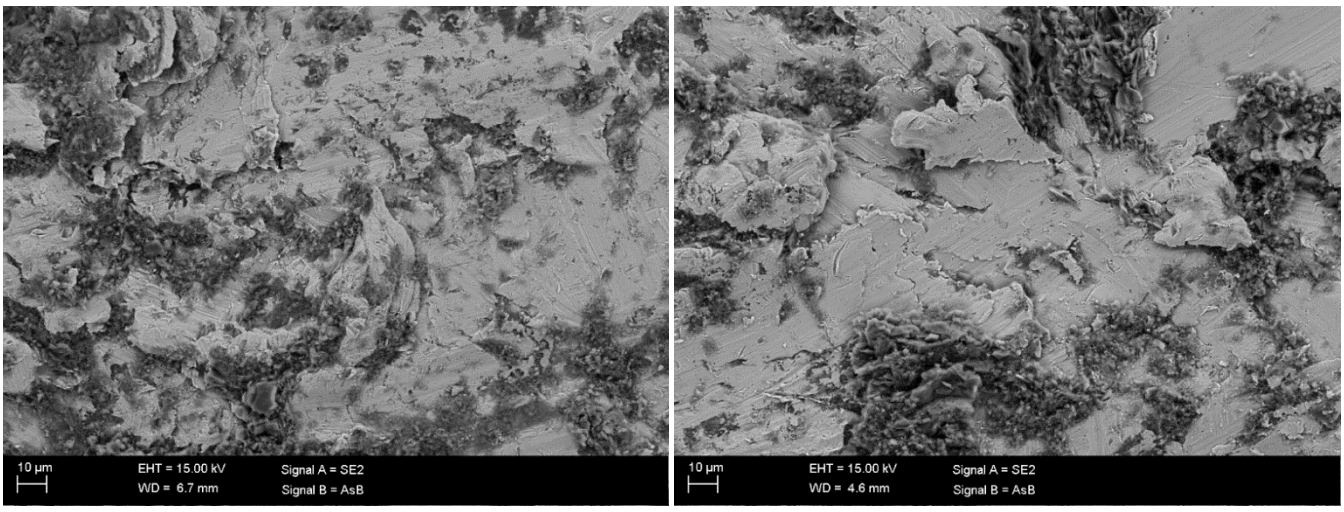

a) *b)*

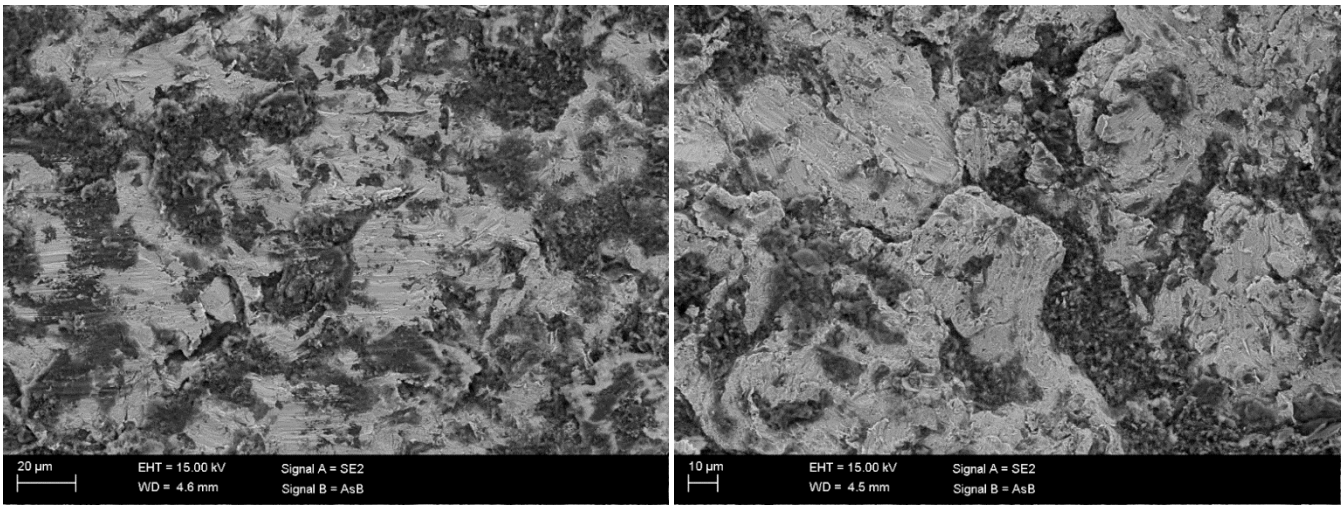

c) *d)*

Fig. 7. SEM images of the B500 steel wear surfaces tested with a) crushing pin-on-disc with a 450HB disc, b) crushing pin-on-disc with a S355 disc, c) dry-pot, and d) impeller-tumbler.

3.4. Characterization of the cross-sections of wear surfaces

Increasing hardness of the steel decreased the deformation depth of the samples in all test types. Fig. 8 shows the cross-sections of samples tested with the dry-pot system, the location from where the images were taken being on the underside of the wear surface about 1 mm from the front edge. The moving direction of the rock in the images is from left to right. The embedded granite abrasives are visible also in the cross-sections, and adiabatic shear bands (ASB) with untempered nanostructured martensite were also occasionally detected on the surfaces. Moreover, the heavy plastic deformation of the steel surface led to the local entrapment of the embedded granite particles, resulting in cracks and delamination of the surface layer.

Fig. 9 presents examples of the B500 steel cross-sections after testing with different test methods. The high-stress abrasion in the crushing pin-on-disc tests produced several micrometers thick layers of embedded rock mixed with steel. These layers, containing also multiple cracks, are prone to fail during continuing wear loading. Both CPOD test procedures produced also some ASBs on the surfaces. In the slurry-pot and impeller-tumbler tests, where the wear mechanism is more of the impact-abrasive type compared to the other methods, occasional subsurface adiabatic shear bands were also formed.

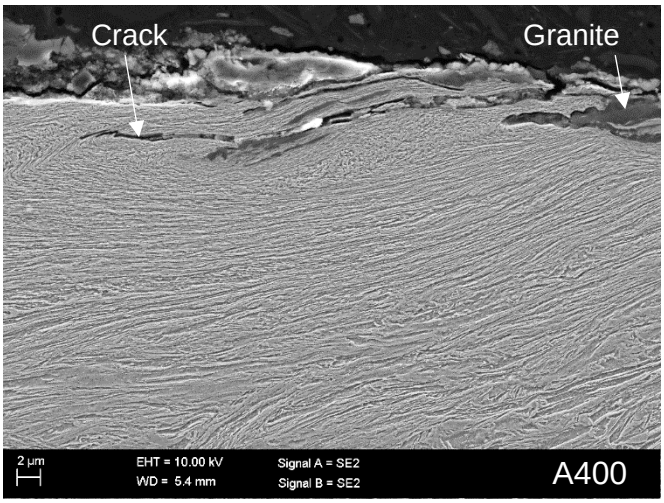

a)

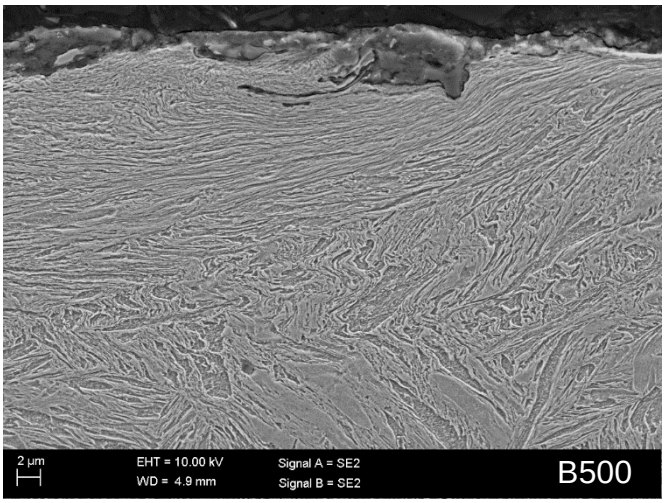

b)

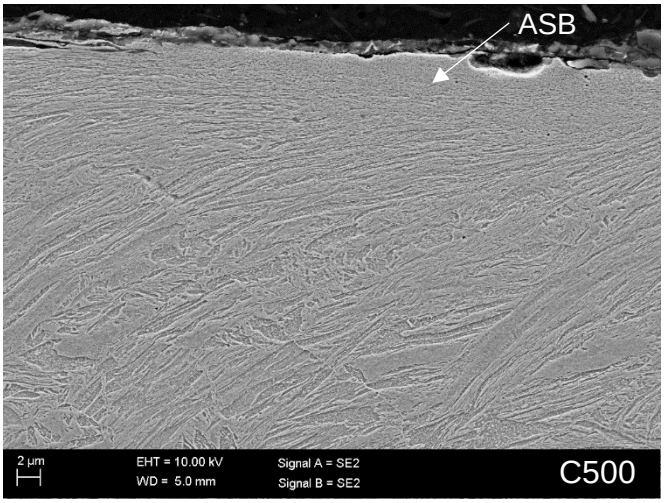

c)

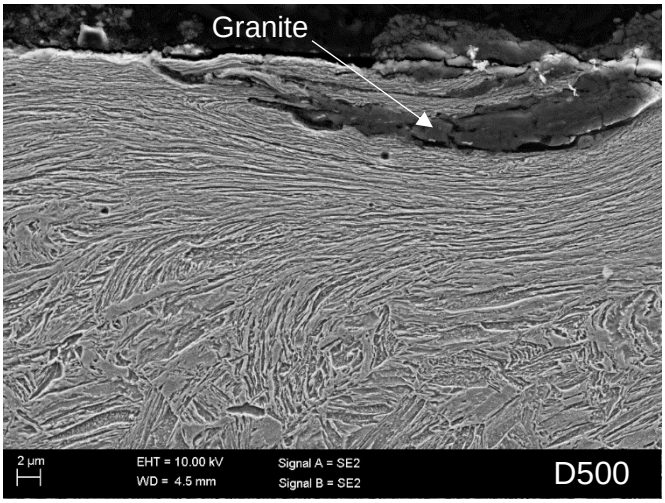

d)

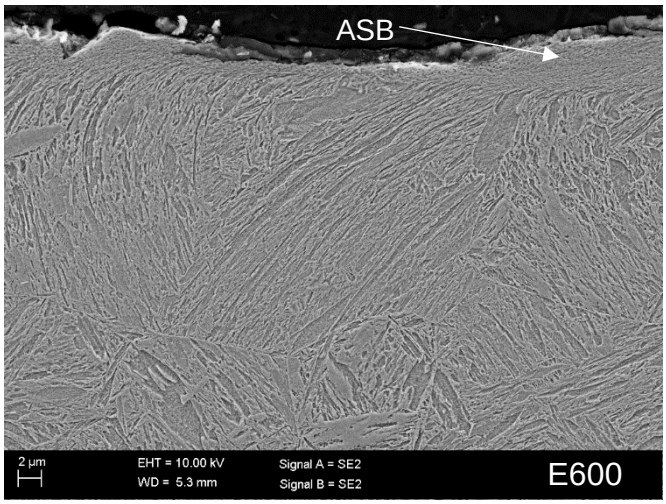

e)

Fig. 8. SEM images comparing the wear surfaces of a) A400, b) B500, c) C500, d) D500, and e) E600 steels tested with the dry-pot method. The abrasives have moved from left to right.

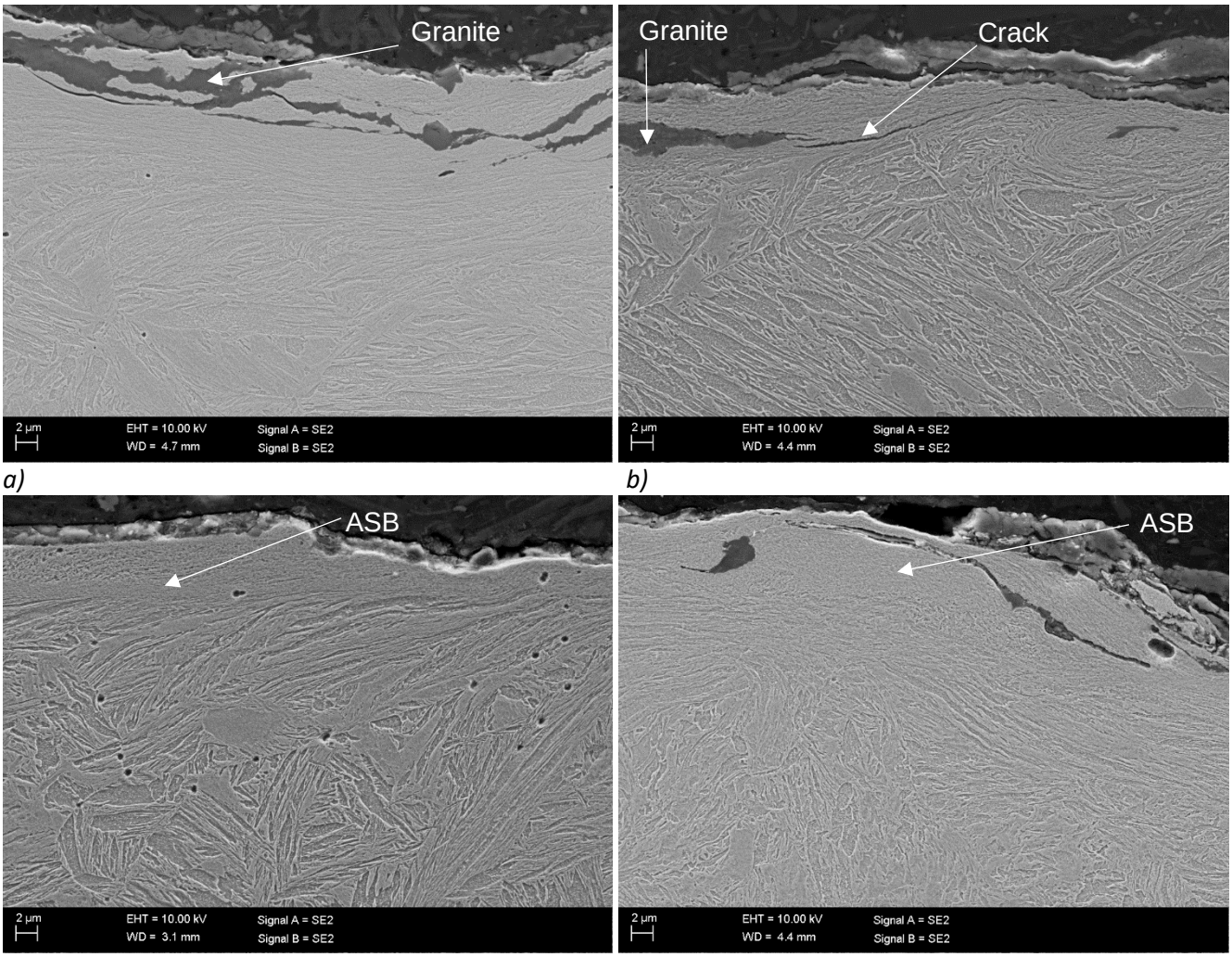

Fig. 9. SEM images of the B500 steel cross-sections tested with a) crushing pin-on-disc with a 450HB disc, b) crushing pin-on-disc with a S355 disc, c) slurry-pot, and d) impeller-tumbler.

The taper sections prepared from the wear surfaces at the tips of the impeller-tumbler samples enabled to study the sub-surface adiabatic shear bands below the actual wear surfaces. Fig. 10 shows two examples of the formed circular ASBs, which are seen as narrow lines in the cross-section images (Figs. 9c and d). In three dimensions, the shapes of the ASBs probably resemble a rotation paraboloid, which is formed during a high strain rate impact by an asperity in a rock. In the taper sections, both the bottom parts and the edges of the formed ASBs were visible. Table 4 presents the median micro hardness values of the formed ASBs and the deformed areas around them. As seen, the severe plastic deformation has markedly work hardened all the studied steels, although the hardness of the deformed areas in the B500 and C500 steels is clearly higher than that of the D500 steel. There was a lot of scatter in the hardness values obtained from the transformed ASB layers, partly because of the difficulties in the actual measurements, but the highest hardness that was measured for the E600 steel was as high as 974 $HV_{0.05}$.

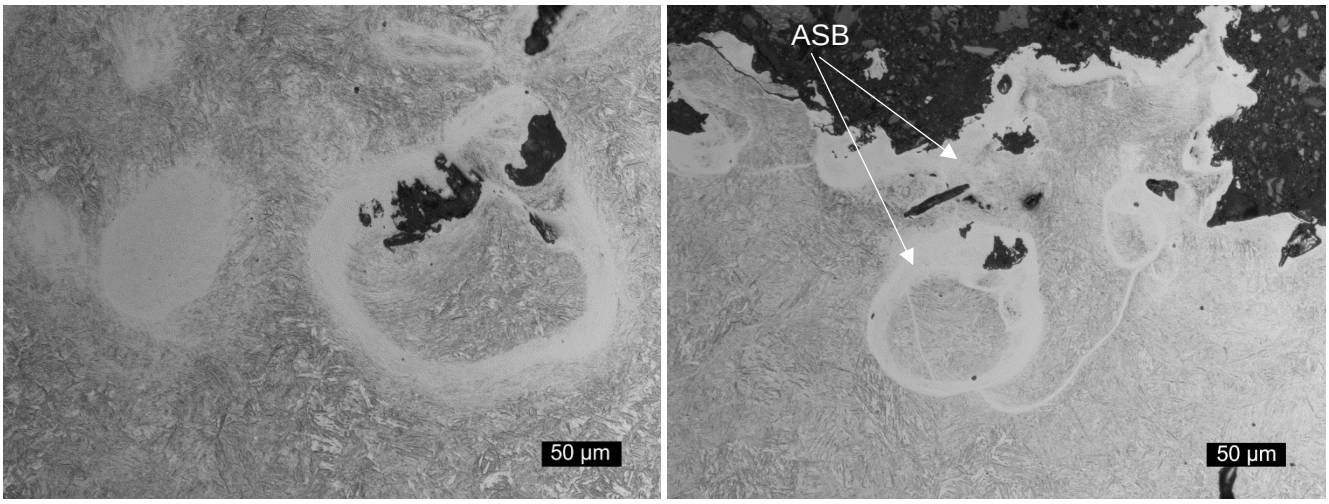

a) *b)*

Fig. 10. Optical micrographs from the taper sections of the tips under the wear surfaces of a) C500 and b) E600 impeller-tumbler samples.

Table 4. Micro hardness of the ASB layers and the deformed areas around them in the impeller-tumbler samples.

Steel	**A400**	**B500**	**C500**	**D500**	**E600**
ASB hardness HV0.05 [kg/mm^2]	718 ± 70	782 ± 33	855 ± 18	749 ± 91	974 ± 16
Deformed hardness HV0.05 [kg/mm^2]	563 ± 48	701 ± 37	693 ± 26	615 ± 46	819 ± 24
Bulk hardness HV10 [kg/mm^2]	421 ± 11	493 ± 6	497 ± 3	486 ± 5	634 ± 5

4. Discussion

The wear mechanisms active in the tests conducted in this work were mostly high-stress abrasion, impact wear, and surface fatigue, all of them occurring simultaneously with different relative proportions. The differences between the test methods were most clearly seen in the determined surface roughness values and in the appearance of the wear surfaces. In the dry-pot method, the freely flowing abrasives did not form as deep scratches as the crushing-pin-on-disc method, where the granite particles are tightly compressed between two steel surfaces. On the other hand, the limited movement of the particles inside the thick gravel bed in the crushing-pin-on-disc tests does not lead to as high energy impacts as in the slurry-pot and impeller-tumbler tests. The embedment of the rock fragments in the wear surfaces was highest in the dry-pot and impeller-tumbler tests. However, the plastic deformation was clearly highest in the impeller-tumbler tested samples, which manifested itself also as a higher surface roughness of the samples.

When abrasive particles plough the surface of a martensitic steel, the material undergoes plastic deformation and usually strain hardens. If the deformability of the surface layer of the material becomes exhausted due to excessive

strain hardening , it may become ‘brittle’ and eventually detaches from the bulk of the material by the continuous abrasive attacks leading to surface fatigue [1,16]. The ability of a steel to deform depends on multiple factors such as the dislocation density, grain size, and internal stresses. Moreover, the impurities in the steel and the amount of inclusions and other material defects may promote the formation of cracks and lead to the eventual deterioration of the wear resistance of the steel. The possible outcomes of ploughing and the resulting effects, such as surface fatigue, depend also on the abrasive material properties and the surrounding system, i.e., on entire tribosystem, which should be carefully accounted for when making materials selections for demanding wear environments.

Previous studies have shown that adiabatic shear bands (also called as white layers) are often formed on the material surfaces during high-stress abrasion [16], while sub-surface ASBs are formed more likely by high-stress/high strain rate impacts [26,27]. The high hardness of the ASBs makes them prone to cracking, which may increase the wear rate in certain conditions [28]. In this study, the surface ASBs were formed only in the crushing-pin-on disc and dry-pot tests, while the subsurface ASBs were formed mostly in the slurry-pot and impeller-tumbler tests.

A martensitic microstructure generally provides good hardness for a steel, and usually the hardness of quenched steels increases with increasing carbon content. The high initial surface hardness is usually beneficial against abrasion, which is also the main reason why the hardest steel E600 showed the lowest mass loss in all of the conducted tests. The combined concentrations of nickel and molybdenum in the B500, C500, and D500 steels were 0.60%, 0.78%, and 0.20%, respectively, while the boron concentrations were similar in the range of 0.0014-0.0019 %. The higher the concentrations of these elements, the better the work hardening ability of the steel is [1]. On the other hand, the total amount of alloying elements was highest in the D500 steel. The micro hardness tests on the deformed layers showed that the strain (work) hardening of the D500 steel was lower than that of the B500 and C500 steels. Thus, the differences in the compositions, which affect the work hardening ability of the steel, may partly explain the higher wear rates of the D500 steel in all test methods compared to the B500 and C500 steels. Moreover, the prior austenite grain size of the D500 steel was smaller than that of the other two HB500 steels, which might also explain the lower work hardening capability of D500. The results indicate that the initial surface hardness of the steel should be high enough to prevent or restrain abrasion, but there should also be some work hardening capability left for the steel to withstand repetitive or continuous ploughing and impacts by the abrasives. The limited work hardening ability of the

already initially hard steels is therefore one of the main explanations for the differences observed in the wear resistance of steels with similar initial (bulk) hardness in the abrasive and impact abrasive conditions.

Although the applied test methods arranged the steels almost in all cases in the same order, the correlation between the test methods was not exactly linear, as illustrated in Fig. 11. For example, the impeller-tumbler produced clearly lower wear rates for the A400 and E600 steels when compared to the other methods. Overall, the lowest wear rates were produced by the crushing pin-on-disc method with a 450HB disc and by the impeller-tumbler method. A similar correlation method between the test types as used in this work was earlier used for example by Tylczak et al. [15], i.e., normalization of the wear rates with the results obtained for a common reference steel. However, the normalization using the actual test parameters shows the true differences between the different test methods and thus, enabled also the comparison of the five methods used in this work.

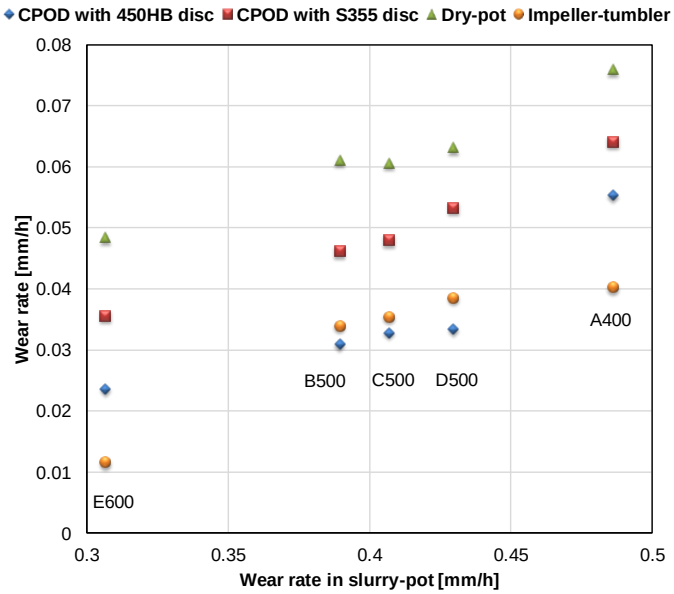

Fig. 11. Correlation between the wear rates (mm/h) in different methods vs. the wear rate in the slurry-pot tests.

The quartzite (or silica sand) used in many low stress methods as a standard mineral has been found largely unsuitable for high-stress abrasion and impact-abrasion testing [16,29,30]. Therefore, a granite abrasive was selected for this study. However, in the tests with natural abrasives, it is important to remember that the properties of the abrasive have a marked effect on the wear test results in any case. The normalization against a reference material reduces the possible small differences between the test batches, especially in the methods that can use a reference material simultaneously with the actual samples, such as the slurry-pot, dry-pot, and impeller-tumbler methods.

It is naturally easier to compare test methods that rely on the same or similar wear mechanisms, test parameters, and contact conditions. For example in the methods used this study, there is a longitudinal wear gradient on the surfaces of the rotating slurry-pot, dry-pot, and impeller-tumbler samples, while in the crushing pin-on-disc samples, the wear rate is more or less uniform over the whole wear surface. Moreover, in the crushing-pin-on-disc tests, the deformation directions change repeatedly because of the freely rotating sample holder. Another major difference is that even though in all the applied test methods the edges of the samples tend to become rounded, in the crushing pin-on-disc tests the edge effect is much smaller compared for example to the impeller-tumbler or slurry-pot tests [31–33].

Although the test equipment and the travel length of the sample edge during the tests were the same, the deformation depth was much higher in the dry-pot tested samples than in the slurry-pot tested samples. The main reason for this is the much higher amount of rock in the dry-pot tests, producing considerably more rock contacts during the tests. However, the three times higher test speed with impact contacts readily explains the higher wear rates observed in the slurry-pot tests. Moreover, the abrasive wear mechanism in the slurry-pot tests included much more cutting than in the dry-pot tests, as revealed by the characterization of the wear surfaces and the determined roughness values.

Conclusions

The wear behavior of five wear resistant steels was studied using different high-stress abrasive and impact-abrasive wear testing methods. From the results of this work, the following conclusions could be drawn:

- The increased work hardening ability of the steel increases its wear resistance in high-stress abrasive and impact-abrasive conditions.
- In high-stress abrasion tests, adiabatic shear bands may form on the wear surfaces. In addition, subsurface ASBs may also form in heavy impact conditions at high strain rates.
- The comparison of different test methods is possible, if the results are normalized against the actual test parameters, such as the wear area and the test time. When comparing the wear rates of materials tested with the same method, normalizing against a reference material should be used, especially when testing with natural abrasives.

- The high-speed slurry-pot produces clearly higher wear rates than the crushing pin-on-disc, the dry-pot, and the impeller-tumbler methods.

Acknowledgements

The work has been done within the DIMECC BSA (Breakthrough Steels and Applications) programme. We gratefully acknowledge the financial support from the Finnish Funding Agency for Innovation (Tekes) and the participating companies. Dr. Vilma Ratia is acknowledged for her assistance with the impeller-tumbler tests.

References

[1] N. Ojala, K. Valtonen, V. Heino, M. Kallio, J. Aaltonen, P. Siitonen, V.-T. Kuokkala, Effects of composition and microstructure on the abrasive wear performance of quenched wear resistant steels, Wear. 317 (2014) 225–232. doi:10.1016/j.wear.2014.06.003.

[2] ASTM G65, Standard Test Method for Measuring Abrasion Using the Dry Sand/Rubber Wheel Apparatus, (2016) 14. doi:10.1520/G0065-16E01.

[3] J.E. Fernández, R. Vijande, R. Tucho, J. Rodríguez, A. Martín, Materials selection to excavator teeth in mining industry, in: Wear, 2001: pp. 11–18. doi:10.1016/S0043-1648(01)00624-X.

[4] R. Dommarco, I. Galarreta, H. Ortíz, P. David, G. Maglieri, The use of ductile iron for wheel loader bucket tips, Wear. 249 (2001) 100–107. doi:10.1016/S0043-1648(01)00531-2.

[5] M.W. Hyttel, D.D. Olsson, G. Reisel, J. Bøttiger, Comparison of a newly developed compression-twist abrasive wear test with the ASTM G65 test method, in: Wear, Elsevier, 2013: pp. 134–141. doi:10.1016/j.wear.2013.08.023.

[6] M. Petrica, C. Katsich, E. Badisch, F. Kremsner, Study of abrasive wear phenomena in dry and slurry 3-body conditions, Tribol. Int. 64 (2013) 196–203. doi:10.1016/j.triboint.2013.03.028.

[7] R. Wilson, J. Hawk, Impeller wear impact-abrasive wear test, Wear. 225–229 (1999) 1248–1257. doi:10.1016/S0043-1648(99)00046-0.

[8] J. Terva, T. Teeri, V.-T. Kuokkala, P. Siitonen, J. Liimatainen, Abrasive wear of steel against gravel with different rock-steel combinations, Wear. 267 (2009). doi:10.1016/j.wear.2009.02.019.

[9] J. Terva, V.-T. Kuokkala, K. Valtonen, P. Siitonen, Effects of compression and sliding on the wear and energy consumption in mineral crushing, Wear. 398–399 (2018) 116–126. doi:10.1016/j.wear.2017.12.004.

[10] N. Ojala, K. Valtonen, P. Kivikytö-Reponen, P. Vuorinen, V.-T. Kuokkala, High speed slurry-pot erosion wear testing with large abrasive particles, Finnish J. Tribol. 33 (2015) 36–44. https://journal.fi/tribologia/article/view/69243.

[11] P.D. Jakobsen, L. Langmaack, F. Dahl, T. Breivik, Development of the Soft Ground Abrasion Tester (SGAT) to predict TBM tool wear, torque and thrust, Tunn. Undergr. Sp. Technol. 38 (2013). doi:10.1016/j.tust.2013.07.021.

[12] J.A. Hawk, R.D. Wilson, J.H. Tylczak, Ö.N. Doğan, Laboratory abrasive wear tests: investigation of test methods and alloy correlation, Wear. 225–229 (1999) 1031–1042. doi:10.1016/S0043-1648(99)00042-3.

[13] J. Allebert, M. Jungedal, P. Waara, Wear on overlay welded HCWI vs. quenched and tempered low alloyed carbon steels evaluated with granite in a laboratory drum test machine, Wear. 330–331 (2015) 364–370. doi:10.1016/J.WEAR.2015.02.059.

[14] M. Varga, High temperature abrasive wear of metallic materials, Wear. 376–377 (2017) 443–451. doi:10.1016/j.wear.2016.12.042.

[15] J.H. Tylczak, J.A. Hawk, R.D. Wilson, A comparison of laboratory abrasion and field wear results, Wear. 225–229 (1999) 1059–1069. doi:10.1016/S0043-1648(99)00043-5.

[16] K. Valtonen, K. Keltamäki, V.-T. Kuokkala, High-stress abrasion of wear resistant steels in the cutting edges of loader buckets, Tribol. Int. 119 (2018) 707–720. doi:10.1016/j.triboint.2017.12.013.

[17] E. Vuorinen, N. Ojala, V. Heino, C. Rau, C. Gahm, Erosive and abrasive wear performance of carbide free bainitic steels - Comparison of field and laboratory experiments, Tribol. Int. 98 (2016) 108–115. doi:10.1016/j.triboint.2016.02.015.

[18] K. Valtonen, Relevance of Laboratory Wear Experiments for the Evaluation of In-Service, Tampere University of Technology, 2018. http://urn.fi/URN:ISBN:978-952-15-4244-2.

[19] A. Sundström, J. Rendón, M. Olsson, Wear behaviour of some low alloyed steels under combined impact/abrasion contact conditions, Wear. 250 (2001) 744–754. doi:10.1016/S0043-1648(01)00712-8.

[20] V. Ratia, K. Valtonen, A. Kemppainen, V.-T. Kuokkala, High-stress abrasion and impact-abrasion testing of wear resistant steels, Tribol. Online. 8 (2013) 152–161. doi:10.2474/trol.8.152.

[21] V. Ratia, V. Heino, K. Valtonen, M. Vippola, A. Kemppainen, P. Siitonen, V.-T. Kuokkala, Effect of abrasive properties on the high-stress three-body abrasion of steels and hard metals, Finnish J. Tribol. 32 (2014) 3–18. https://journal.fi/tribologia/issue/view/3255.

[22] N. Ojala, K. Valtonen, A. Antikainen, A. Kemppainen, J. Minkkinen, O. Oja, V.-T. Kuokkala, Wear performance of quenched wear resistant steels in abrasive slurry erosion, Wear. 354–355 (2016) 21–31. doi:10.1016/j.wear.2016.02.019.

[23] V. Ratia, I. Miettunen, V.-T. Kuokkala, Surface deformation of steels in impact-abrasion: The effect of sample angle and test duration, Wear. 301 (2013) 94–101. doi:10.1016/j.wear.2013.01.006.

[24] R.L. Higginson, C.M. Sellars, Worked examples in quantitative metallography, Maney, London, 2003.

[25] V. Ratia, Behavior of Martensitic Wear Resistant Steels in Abrasion and Impact Wear Testing Conditions, Tampere University of Technology, 2015. http://urn.fi/URN:ISBN:978-952-15-3627-4.

[26] K. Valtonen, V. Ratia, K.R. Ramakrishnan, M. Apostol, J. Terva, V.-T. Kuokkala, Impact wear and mechanical behavior of steels at subzero temperatures, Tribol. Int. (2018). doi:10.1016/J.TRIBOINT.2018.08.016.

[27] E. Abbasi, Q. Luo, D. Owens, Case study: Wear mechanisms of NiCrVMo-steel and CrB-steel scrap shear blades, Wear. 398–399 (2018) 29–40. doi:10.1016/j.wear.2017.11.014.

[28] Y.Y. Yang, H.S. Fang, W.G. Huang, A study on wear resistance of the white layer, Tribol. Int. 29 (1996) 425–428. doi:10.1016/0301-679X(95)00099-P.

[29] J.D. Gates, M.S. Dargusch, J.J. Walsh, S.L. Field, M.J.P. Hermand, B.G. Delaup, J.R. Saad, Effect of abrasive mineral on alloy performance in the ball mill abrasion test, Wear. 265 (2008) 865–870. doi:10.1016/j.wear.2008.01.008.

[30] E. Albertin, A. Sinatora, Effect of carbide fraction and matrix microstructure on the wear of cast iron balls tested in a laboratory ball mill, Wear. 250–251 (2001) 492–501. doi:10.1016/S0043-1648(01)00664-0.

[31] J. Terva, V.-T. Kuokkala, P. Kivikytö-Reponen, The edge effect of specimens in abrasive wear testing, Finnish J. Tribol. 31 (2012) 27–35. https://journal.fi/tribologia/article/view/69339.

[32] V. Ratia, K. Valtonen, A. Kemppainen, V.-T. Kuokkala, The Role of Edge-Concentrated Wear in Impact-Abrasion Testing, Tribol. Online. 11 (2016) 410–416. doi:10.2474/trol.11.410.

[33] N. Ojala, K. Valtonen, J. Minkkinen, V.T. Kuokkala, Edge and particle embedment effects in low- and high-stress slurry erosion wear of steels and elastomers, Wear. 388–389 (2017) 126–135. doi:10.1016/j.wear.2017.06.004.